

# Peculiar nature of hard X-ray eclipse in SS433 from INTEGRAL observations

A.M. Cherepashchuk<sup>1</sup>, R.A. Sunyaev<sup>2</sup>, K.A. Postnov<sup>1</sup>, E.A. Antokhina<sup>1</sup>,  
S.V. Molkov<sup>2,3</sup>  $\star$

<sup>1</sup>*Sternberg Astronomical Institute, Universitetskij pr. 13, Moscow 119992, Russia*

<sup>2</sup>*Space Research Institute, Moscow, Russia*

<sup>3</sup>*CESR, Toulouse, France*

Accepted ..... Received .....; in original form .....

## ABSTRACT

The analysis of hard X-ray INTEGRAL observations (2003–2008) of superaccreting galactic microquasar SS433 at precessional phases of the source with the maximum disk opening angle is carried out. It is found that the shape and width of the primary X-ray eclipse is strongly variable suggesting additional absorption in dense stellar wind and gas outflows from the optical A7I-component and the wind-wind collision region. The independence of the observed hard X-ray spectrum on the accretion disk precessional phase suggests that hard X-ray emission (20 – 100 keV) is formed in an extended, hot, quasi-isothermal corona, probably heated by interaction of relativistic jet with inhomogeneous wind outflow from the precessing supercritical accretion disk. A joint modeling of X-ray eclipsing and precessional hard X-ray variability of SS433 revealed by INTEGRAL by a geometrical model suggests the binary mass ratio  $q = m_x/m_v \simeq 0.25 \div 0.5$ . The absolute minimum of joint orbital and precessional  $\chi^2$  residuals is reached at  $q \simeq 0.3$ . The found binary mass ratio range allows us to explain the substantial precessional variability of the minimum brightness at the middle of the primary optical eclipse. For the mass function of the optical star  $f_v = 0.268M_\odot$  as derived from Hillwig & Gies data, the obtained value of  $q \simeq 0.3$  yields the masses of the components  $m_x \simeq 5.3M_\odot$ ,  $m_v \simeq 17.7M_\odot$ , confirming the black hole nature of the compact object in SS433.

**Key words:** X-rays: binaries — X-rays: SS433 — binaries: eclipsing

## 1 INTRODUCTION

SS433 is a massive close binary system at advanced evolutionary stage (Margon 1984; Cherepashchuk 1981, 1989; Fabrika 2004). This unique galactic X-ray binary with precessing relativistic jets ( $v = 0.26c$ , where  $c$  is the speed of light) exhibits several variabilities, including the precessional one (with the period  $P_{prec} \simeq 162$  d), the eclipsing one (with the binary orbital period  $P_{orb} \simeq 13.08$  d), and the nutational one (with the nutation period  $P_{nut} \simeq 6.28$  d) (e.g. Goranskij et al. (1998), Davydov et al. (2008)). SS433 is recognized as a galactic microquasar with precessing supercritical accretion disk around a compact object, and has been extensively investigated in the optical, radio and X-ray ranges (for a comprehensive review and references see Fabrika (2004)). Recent high-resolution optical spectroscopy of the system (Hillwig & Gies 2008) revealed the presence of absorption lines in the spectrum of the optical component identified as a  $\sim$  A7I supergiant star. Observed orbital Doppler shifts of the absorption lines of the optical component and stationary HeII emission allowed Hillwig & Gies to determine the mass ratio of the compact ( $m_x$ ) and the optical ( $m_v$ ) components in SS433  $q = m_x/m_v \simeq 0.35$ , implying the binary masses  $m_x = 4.3 \pm 0.8M_\odot$  and  $m_v = 12.3 \pm 3.3M_\odot$ . Similar values of  $q$ ,  $m_x$  and  $m_v$  were obtained from the analysis of the optical light curves of SS433 (Antokhina & Cherepashchuk 1987).

The analysis of broad X-ray eclipses in the 1-10 keV range observed by *ASCA* and *Ginga* satellites suggests a smaller mass ratio than that obtained from optical spectroscopy and photometry. For example, using X-ray eclipses observed by *Ginga* Brinkman et al. (1989) estimated  $q \simeq 0.15$ . In their analysis, the authors used the simplifying assumption that the X-ray source is compact and the duration of the X-ray eclipse is fully determined by the size of the optical companion. *Ginga* light curves at different precessional phases presented in Kawai et al. (1989) were analyzed by Antokhina et al. (1992) using the method of binary light curve synthesis in the model including the precessing accretion disk and jets. They found the possible range of binary mass ratios  $q = 0.15 - 0.25$ . Using X-ray emission from SS433 observed by the *ASCA* satellite (which is mostly produced in precessing thermal jets), Kotani (1998) and Kotani et al. (1998) estimated  $q \simeq 0.22$ . Their analysis, with account of uncertainties, allowed in fact a fairly broad range of binary mass ratios  $q = 0.06 - 0.31$ .

\* E-mail: cherepashchuk@gmail.com(AMCh); kpostnov@gmail.com(KAP); elant@sai.msu.ru(EAA)

Thus the average mass ratio estimate as inferred from the analysis of 1-10 keV X-ray data is smaller ( $q \leq 0.25$ ) than that inferred from optical observations ( $q \sim 0.35$ ). However, for  $q < 0.25$  the total eclipse of the accretion disk by the optical star must occur, so it is hard to explain a significant optical variability of SS433 in the primary eclipse minimum with precessional phase, as in fact observed (Goranskij et al. 1998).

The INTEGRAL satellite detected the hard X-ray emission from SS433 up to 100 keV (Cherepashchuk et al. 2003). Our studies of SS433 based on the INTEGRAL observations suggested the presence of a hot rarefied corona above the supercritical accretion disk in this source (Cherepashchuk et al. 2005, 2007). The peculiar variability in the shape and width of the primary eclipse in hard X-rays was discovered. The spectral analysis of archival RXTE observations of SS433 (Filippova et al. 2006) found evidence for strong variable X-ray absorption which does not support the assumption that the optical star can be considered as an opaque screen with sharp edges at these energies. This implies that the primary eclipse in SS433 is not purely geometrical and that the binary mass ratio as inferred from the analysis of the *Ginga* and *ASCA* data may suffer from systematic uncertainties.

The results of our previous analysis of the orbital and precessional variability in SS433 observed by INTEGRAL (Cherepashchuk et al. 2005, 2007) can be summarized as follows. The hard X-ray flux (25-50 keV) from the source clearly exhibits variability with the precessional period  $P_{prec} \simeq 162.4$  d from  $\sim 3$  mCrab at the cross-over phase to  $\sim 18 - 20$  mCrab at the maximum disk opening phase (the  $T_3$  moment, where the moving emission lines in the SS433 spectrum are at maximum separation). Eclipses are observed with the orbital period  $P_{orb} \simeq 13.08$  d and are very significant. Eclipses observed close to the  $T_3$  phase (at the precessional phase  $\psi \simeq 0$ ) are the deepest ones. The hard X-ray flux (18-60 keV) at the center of the primary eclipse is still detectable at a level of  $\sim 3$  mCrab, so the ratio of the maximum uneclipsed flux ( $\sim 20$  mCrab) to the minimum flux value at the mid-eclipse is about 6-7, which is similar to the amplitude of the precessional off-eclipse hard X-ray variability. The width of the hard X-ray eclipse is found to be larger than that in soft X-rays. The egress out of the hard X-ray eclipse is observed to be strongly variable, most probably due to absorption of the X-ray flux by accretion flows and asymmetric structured wind from the supercritical accretion disk and by the wind-wind collision region. Similar distortions of the eclipse egress were first observed by *Ginga* (18.4-27.6 keV) (Kawai et al. 1989). The hard X-ray spectrum (20-200 keV) does not noticeably change with precessional phase. All these facts suggest that most of the hard X-ray flux of SS433 is generated in a hot extended

corona formed in the central parts of the accretion disk. The hot corona may be formed as a result of collision of the wind inhomogeneities with relativistic jets (Begelman et al. 2006). A more detailed interpretation of the broad-band (3-90 keV) X-ray continuum of SS433 in terms of the multicomponent model including the accretion disk, jet and corona has been carried out by Krivosheyev et al. (2009).

In the present paper, we analyze INTEGRAL observations of hard X-ray eclipses of SS433 near the T3 moment and interpret them in terms of our multicomponent geometrical model with account of the peculiar shape and strong variability of the primary eclipse and precessional X-ray variability of the source. In Section 2 we describe INTEGRAL observations used for the analysis. In Section 2.1 we discuss the precessional variability of SS433. In Section 2.2 we present IBIS/ISGRI spectra of SS433 obtained at different precessional intervals and show that they can be fitted by one power law. In Section 2.3 we study in more detail the primary eclipse of SS433 in hard X-rays. Section 3.1 depicts our geometrical model. In Section 3.2 the best-fit mass ratio is obtained from joint analysis of eclipsing and precessional light curves. We discuss the obtained results in Section 4 and summarize our findings in Section 5.

## 2 OBSERVATIONS

Dedicated INTEGRAL observations of SS433 were carried out in AO-1 for 500 ks, in AO-3 for 500 ks, in AO-4 for 466 ks, in AO-5 for  $\sim 900$  ks and in AO-6 for  $\sim 500$  ks. The AO-1 observations (INTEGRAL orbits 67-69) were performed at the precessional phase 0 with maximum disk opening. In AO-2, SS433 fell within the FOV of IBIS when observing the Sagittarius Arm Tangent region, but no X-ray eclipses occurred during this program. In AO-3, SS433 was observed around different precessional phases (INTEGRAL orbits 366-369). One X-ray eclipse was partially measured again at the precessional phase close to zero, with an indication of a much narrower eclipse or a sudden mid-eclipse (at the orbital phase  $\phi \sim 1.03$ ) flux increase. Based on these data, the model for the source eclipse has been constructed in (Cherepashchuk et al. 2005, 2007); however, these data were not strongly constrained by precessional variability and allowed a broad range of the binary mass ratio  $q \sim 0.1 - 0.5$ . In AO-4, the source was observed in May 2007; unfortunately, due to high variability, the source flux was very low, so we exclude these data from the analysis of X-ray eclipses (set II in Fig. 5 below). Note the strong increase in the apparent eclipse width. In

AO-5, two consecutive eclipses of the source near the zero precessional phase  $\psi = 0$  were observed in October 2007. Adding all of these observations allowed us to construct hard X-ray spectra of the source at different precessional phases (Fig. 4). However, the statistics is still insufficient to make orbital phase-resolved spectroscopy. In AO-6, the egress out of the primary eclipse of SS433 was observed in September 2008 (set V in Fig. 5 below).

The INTEGRAL data were processed with both publically available ISDC software (OSA-7 version) and the original software package written by the IKI INTEGRAL team (for the IBIS/ISGRI telescope, see (Molkov et al. 2004) for more detail). For the analysis of precessional variability of SS433 we have used both data from our INTEGRAL observing program of SS433 and publically available data of all observations where the source was in the FOV of the IBIS/ISGRI telescope ( $< 13$  degrees). The total exposure of the selected data is approximately 8.5 Ms. To perform precessional phase-resolved analysis we ascribed to each SCW (Science Window or SCW, the natural piece of INTEGRAL data – pointing observation with an exposure of  $\sim 2 - 5$  ks) the appropriate orbital and precessional phases. The phases are calculated using the ephemeris provided by Fabrika (2004). The orbital primary minimum (corresponding to  $\phi = 0$ ) is

$$JD_{MinI}(\text{hel}) = 2450023.62 + 13.08211 \times E,$$

the zero precession phase (corresponding to the T3 moment,  $\psi = 0$ ) is

$$JD_{T3}(\text{hel}) = 2443507.47 + 162.375 \times E1.$$

In Fig. 1 (left panels) we show the exposure distribution of the used observations by phases. For clarity we presented two cycles. The exposure time distribution over orbital phases is distributed more or less homogeneously, while that over precessional phases shows an excess near the T3 moment, since the main part of our SS433 INTEGRAL observing program was focused on observations of the primary eclipses at zero precessional phases where the source flux is maximal.

## 2.1 Precessional variability

In this Section we focused on the precessional phase-resolved analysis of SS433. To exclude the orbital modulation, we have used only observations at orbital phases from the range  $0.3 < \phi < 0.7$ . After this filtering we still have  $\sim 2.8$  Ms of data distributed across all precessional phases, as shown in Fig. 1 (the right panel).

The combined AO1 – AO5 data (including those publically available) enabled us to

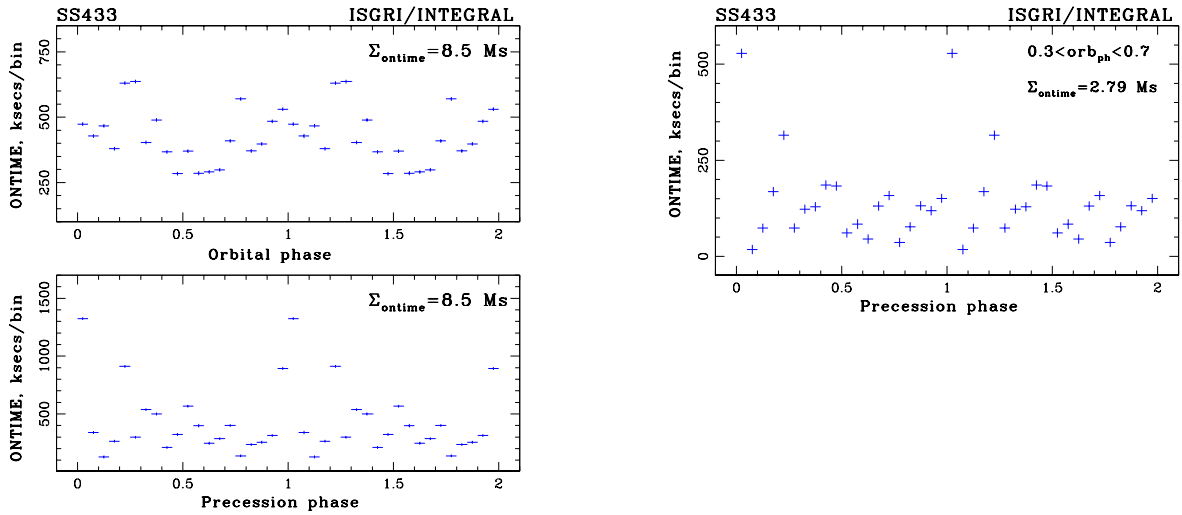


**Figure 1.** Left panel: distribution of the observing time of SS433 by the orbital (upper) and the precession (bottom) phases. Right panel: the distribution of the duration of the off-eclipse data ( $0.3 < \psi_{orb} < 0.7$ ) over precessional phase used for the construction of the precessional light curve.

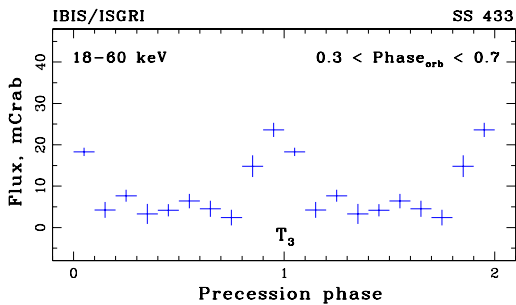


**Figure 2.** Average precessional light curve of SS433 from all available IBIS/ISGRI 18-60 keV data. Orbital eclipses are excluded.

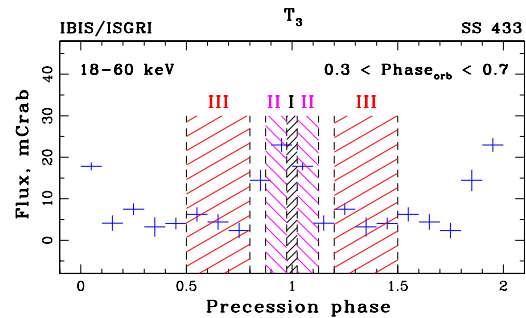


**Figure 3.** Precessional phase intervals chosen for spectral analysis of SS433.

measure, for the first time, the precessional hard X-ray variability (Fig. 2,3), which turned out to be quite significant and stable over several precessional periods. The maximum to minimum flux ratio of the average precessional variability is around 5-7, which is higher than in softer X-ray bands, and suggests the hard X-ray emission originating closer to the base of the visible part of the jets. The eclipsing and precessional variabilities, combined with spectroscopic data simultaneously taken with INTEGRAL observations by the 6-m telescope SAO RAS, were taken into account when attempting to model the light curve of the source by (Cherepashchuk et al. 2005). However, the results proved to be inconclusive. First of all, the spectral resolution of the optical observations (around 3000) was insufficient

to definitely measure the radial velocity curve of the optical companion. The modeling of X-ray eclipse and precessional variability allowed fairly broad range of parameters, including the mass ratios  $q \sim 0.1 - 0.5$  (primarily due to the lack of reliable observations at the middle of the hard X-ray eclipse). An independent spectral analysis of archival RXTE observations of SS433 (Filippova et al. 2006) also suggested that it is hard to derive the binary mass ratio based on X-ray eclipse observations only.

## 2.2 Hard X-ray spectra

Our previous studies (Cherepashchuk et al. 2003, 2005, 2007) suggested that SS433 is a superaccreting galactic microquasar with hot corona above the accretion disk which scatters hard X-ray radiation from the central parts of the disk. Out of the eclipse, the source has been reliably detected by IBIS/ISGRI telescope up to 100 keV, with the X-ray continuum fitted by a featureless power-law  $dN/dt/dA/dE \sim E^{-2.8}$  ph/s/cm<sup>2</sup>/keV (Cherepashchuk et al. 2003, 2005, 2007), see Fig. 4.

INTEGRAL observations (2003-2007) were separated into three segments in the precessional phase (Fig. 3) (limited by photon statistics). The resulted spectra are shown in Fig. 4, with no clear difference in the power-law fit in the 20-100 keV energy band. It is recognized from RXTE observations that at softer X-ray band the spectrum is very variable (Filippova et al. 2006), but errors in the first point 18-22 keV of our fit which can be due to this variability have no effect on the value of the power-law fit. One hard X-ray spectral fit at different precessional phases of the accretion disk suggests the presence of a fairly broad hard X-ray emission region. To be independent of the disk opening angle varying with the precessional phase, the size of this region must be comparable to that of the accretion disk ( $10^{11} - 10^{12}$  cm).

The X-ray continuum spectrum of SS433 in the broad range 3-100 keV can be fitted by a two-component model including thermal X-ray emission from the cooling jet and thermal comptonization spectrum from the isothermal corona Krivosheyev et al. (2009). For both uneclipsed and partially eclipsed by the accretion disk corona the model gives the best spectral fits for  $T_{cor} \simeq 20$  keV with Thomson optical depth  $\tau_T \simeq 0.2$ , the mass outflow rate in the jet  $\dot{M}_j \simeq 3 \times 10^{19}$  g/s corresponding to a jet kinetic power of  $\sim 10^{39}$  erg/s. These parameters suggest an electron density of  $\sim 5 \times 10^{12}$  cm<sup>-3</sup> at distances  $\sim 5 \times 10^{11}$  cm. Such a density is typical in the wind outflowing with velocity  $v \sim 3000$  km/s from a supercritical

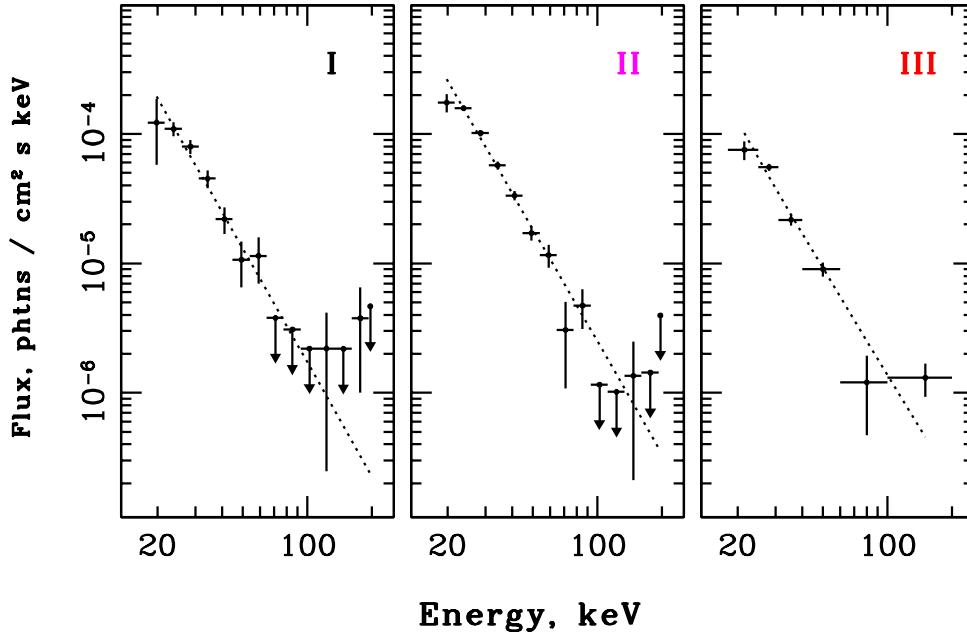


**Figure 4.** IBIS/ISGRI 10 – 200 keV SS433 spectra at different precessional phases. From left to right: spectra averaged inside phase intervals I, II, III shown in Fig. 3, respectively. All spectra can be fitted by a power-law model with the photon spectral index  $-2.8$  (the dotted line).

accretion disk with  $\dot{M} \sim 10^{-4} M_{\odot}/\text{yr}$  at distances  $\sim 10^{11} - 10^{12}$  cm from the center, where the Compton-thick photosphere is formed (Fabrika 2004; Revnivtsev et al. 2004).

Note that despite several primary eclipses have already been observed by INTEGRAL, the measured hard X-ray flux  $\sim 5 - 20$  mCrab from the source is still insufficient for phase-resolved spectral analysis of an individual eclipse. To this aim, additional observations of SS433 by INTEGRAL are planned.



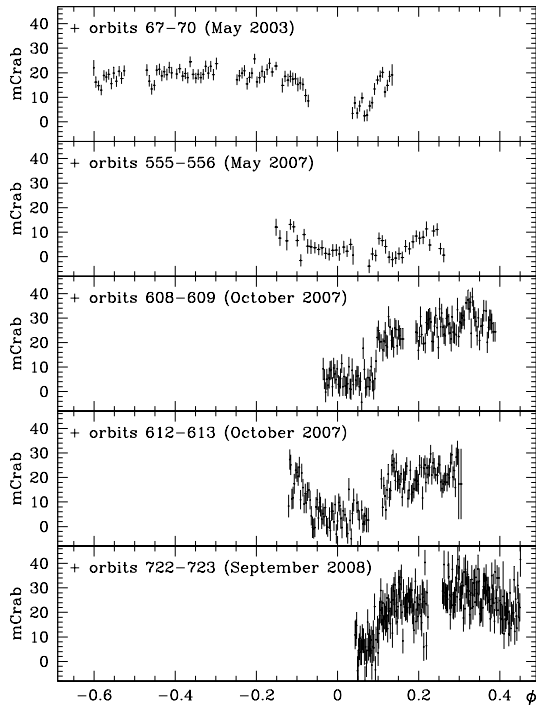


**Figure 5.** From top to bottom: primary eclipses of SS433 observed by INTEGRAL (IBIS/ISGRI data, 18-60 keV) during I, II, III, IV and V sets (see the text).

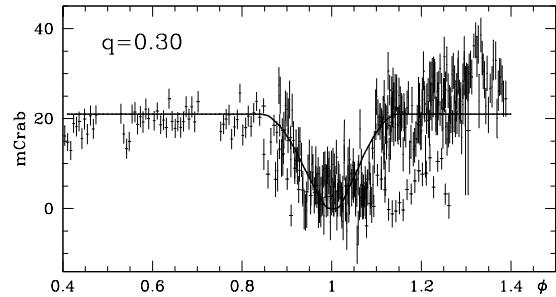


**Figure 6.** Combined I-IV INTEGRAL primary eclipses of SS433. The solid curve shows the model light curve for  $q = 0.3$  (see the text).

### 2.3 The primary eclipse and its peculiarity

The dedicated INTEGRAL observations of the primary eclipses of SS433 in 2003, 2007 and 2008 were obtained near the  $T3$  precessional phase when the accretion disk is maximally open. The data include:

- I. INTEGRAL orbits 67-70 (May 2003), precessional phase  $\psi = 0.001 - 0.060$ ;
- II. INTEGRAL orbits 555-556 (May 2007), precessional phase  $\psi = 0.980 - 0.014$ ;
- III. INTEGRAL orbits 608-609 (October 2007), precessional phase  $\psi = 0.956 - 0.990$ ;
- IV. INTEGRAL orbits 612-613 (October 2007), precessional phase  $\psi = 0.030 - 0.064$ .
- V. INTEGRAL orbits 722-723 (September 2008), precessional phase  $\psi = 0.057 - 0.091$ .

The observed eclipses are shown in Fig 5. In our analysis we have used only sets I, III, IV, V and excluded set II (the one showing the most suppressed egress out of the primary eclipse).

SS433 is known to be a highly variable object at all wavelengths (Cherepashchuk 1989; Fabrika 2004; Revnivtsev et al. 2004, 2006). This is not surprising for a supercritically accreting massive binary, considering various instabilities that should be immanently present in the mass outflow from the optical star and in the accretion disk. It might appear that the primary eclipse of the hard X-ray emission coming from the regions close to the central

black hole by the optical star should be stable. However, it is not the case for hard X-ray eclipse in SS433 (Fig. 5). As seen in this figure, the second eclipse observed in May 2007 (INTEGRAL orbits 555-556) has an unusually broad form: a shallow ingress to and broad egress from the eclipse, which may be due to the low level of uneclipsed X-ray flux from the source  $\sim 10$  mCrab. Note that this particular eclipse is very similar to the one observed by *Ginga* (Kawai et al. 1989). However, already at the next T3 moment in October 2007 (sets III and IV in Fig. 5) the uneclipsed X-ray flux was at a level of 20 mCrab and the egress from eclipse restored its more familiar form (like in set I). This effect is particularly clearly visible on the combined X-ray eclipse light curve shown in Fig. 6. The reason for such a strong variability of the hard X-ray egress may be related to powerful inhomogeneous gaseous streams feeding the disk and the wind from the supercritical accretion disk. Additional X-ray absorption can be produced in the collision region of the winds from the optical star and the supercritical accretion disk (Cherepashchuk et al. 1995).

The slow dense wind from the accretion disk in SS433 should form a Compton-thick photosphere and funnels around relativistic jets (Fabrika 2004). The height of the funnel  $\sim 10^{12}$  cm, comparable to the accretion disk size, can be inferred from the observed  $\sim 80$ -s lag of the optical emission with respect to the X-rays from the jet base found in the simultaneous optical/X-ray observations of the source (Revnivtsev et al. 2004). Thus it appears quite possible that the variable wind from the precessing supercritical accretion disk causes changes of the funnel structure, so even at the maximum opening disk phase (T3) the shape of hard X-ray eclipse may appreciably vary depending on the accretion rate through the disk. In this connection it is worth noticing the variable broad absorption-like feature that appears immediately after the egress from the eclipse (at orbital phases  $\phi \sim 0.15 - 0.2$ , see Fig. 5). It would be very interesting to know whether this feature is due to the true absorption of X-ray emission or just reflects the strong variability of the proper X-ray flux.

We conclude that the hard X-ray eclipse in SS433 is likely to be formed by both geometrical screening of the broad X-ray emitting region by the opaque star and complex gaseous stream and/or inhomogeneous wind from the optical star and the supercritical accretion disk, as well as by the wind-wind collision region. This implies that when fitting the hard X-ray primary eclipse in SS433 by geometrical model, we should use the most stable part of the observed eclipses, i.e. the ingress to the eclipse and the *upper envelope* of the observed egress out of eclipse. In view of high variability, the analysis of one individual X-ray eclipse only can lead to erroneous determination of the binary system parameters. Moreover, for

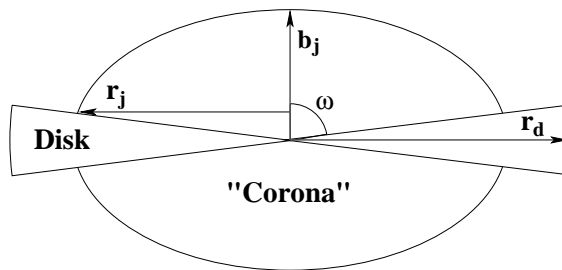


**Figure 7.** Geometrical model of the accretion disk and its "corona".

their reliable determination a joint modeling of both orbital and precessional variability of hard X-ray flux is needed.

### 3 ANALYSIS OF HARD X-RAY LIGHT CURVES OF SS433

#### 3.1 Geometrical model of SS433

To analyze hard X-ray eclipses of SS433 we used a geometrical model developed earlier for the interpretation of the *Ginga* data (Antokhina et al. 1992) and the *INTEGRAL* light curve (Cherepashchuk et al. 2005). We consider a close binary system consisting of an (opaque) "normal" star limited by the Roche equipotential surface and a compact object surrounded by an optically and geometrically thick "accretion disk". Relativistic jets are directed perpendicularly to the disk plane. The "accretion disk" includes the disk itself and an extended photosphere formed by the outflowing wind. The orbit is circular, the axial rotation of the normal star is assumed to be synchronized with the orbital revolution.

The disk and "jets" are precessing in space and change the orientation relative to the normal (donor) star. The disk is inclined with respect to the orbital plane by the angle  $\theta$ . A cone-like funnel is located inside the disk and is characterized by the half-opening angle  $\omega$ , thus the opaque disk body (see Fig. 7) is described by the radius  $r_d$  and the angle  $\omega$ . The central object is surrounded by a transparent quasi-isothermal homogeneously emitting spheroid with a visible radius  $r_j$  and height  $b_j$  which could be interpreted as a "corona" or a "thick jet" (without any relativistic bulk motion). Here  $r_j$ ,  $b_j$  and  $r_d$  are dimensionless values expressed in units of the binary separation  $a$ . The radius of the normal star is determined by the relative Roche lobe size, i.e. by the mass ratio  $q = m_x/m_v$  ( $m_x$  is the mass of the compact object).

Only the "corona" is assumed to emit in the hard X-ray band, while the star and disk

eclipse it in the course of the orbital and precessional motion. During precession the inclination of the disk with respect to the observer changes, causing different visibility conditions for the "corona". The "corona" is partially screened by the cone disk edge, which can explain qualitatively the change of the uneclipsed X-ray flux with precession phase. Observations of the precessional variability can thus be used to obtain a "vertical" scan of the emitting structure, restricting the parameters  $b_j$  and  $\omega$ . The orbital (eclipse) variability observations scan the emitting structure "horizontally", restricting possible values of  $r_d$ ,  $\omega$ ,  $q$  and  $r_j$ . The joint analysis of the precessional and eclipse variability thus enables us to reconstruct the spatial structure of the accretion disk central region, where the hard X-rays are produced, and to estimate the binary mass ratio  $q$ .

The position of the components of the system relative to the observer is determined by the binary orbit inclination angle  $i = 78.8^\circ$ , the disk inclination angle to the orbital plane  $\theta = 20.3^\circ$  (Margon 1984; Davydov et al. 2008), and the precessional phase  $\psi$ .

### 3.2 Results of light curves analysis

Our model for the orbital and precessional variability of SS433 has the following free parameters: the binary mass ratio  $q = m_x/m_v$  determining the relative size of the normal star, the disk parameters  $r_d, \omega$  determining the form of the disk, the thick "jet" or "corona" parameters  $r_j, b_j$  determining the form of the hot corona. Note that the X-ray emitting region is qualitatively different for a thin narrow "jet" with  $r_j \ll b_j \sim a$  and a thin short "jet" with  $r_j \ll b_j \ll a$ . If  $r_j > b_j$ , it is more appropriate to term it as a corona (or a thick "jet"). For each value of  $q$  from the range 0.05 – 1.0, we found other parameters best-fitting simultaneously the orbital and precessional light curves. We remind that the precessional light curve was constructed using maximum off-eclipse X-ray flux from the system. The precessional variability amplitude was assumed to be  $A_{pr} \simeq 5 - 7$ . The  $\chi^2$  criterion was used to evaluate the goodness of fits.

To examine as fully as possible the binary system parameters, we have used different variants of modeling of the observed orbital hard X-ray variability. These included:

- 1) the analysis of light curves consisting of individual points;
- 2) the analysis of average light curves;
- 3) the analysis of individual observational sets (I, III, and IV-V);
- 4) the analysis of the combined data from sets I, III and IV-V;

5) the analysis of the entire eclipse, including the eclipse ingress and (the upper envelope of) egress;

6) the analysis of the ingress to the eclipse only (orbital phases  $\psi_{orb} = 0.8 - 1.0$ ).

All methods give similar results. The inferred binary system parameters are found to be sensitive mostly to the form of ingress and the duration of the primary eclipse. The results of the analysis can be summarized as follows.

1) The analysis of individual and average light curves yields similar results (i.e. the use of the average light curve does not add errors to the obtained parameters). This might seem obvious, but we directly checked it.

2) The analysis of individual data sets I, III, IV, V and the combined data yields similar results.

Taking into account the above conclusions, below we shall show the model light curve for the combined data sets I, III, IV and V.

3) When searching for the best-fit model parameters at different  $q$ , we found that solutions obtained for the entire primary eclipse (the ingress and the upper envelope of egress) and for the eclipse ingress only are not very different. Taking into account highly variable character of the eclipse egress noted above, below we shall discuss solutions and model parameters obtained from the analysis of the *eclipse ingress part only*. In the combined primary eclipse (Fig. 6) the ingress part is mostly determined by sets I and IV.

4) In our previous analysis of the primary orbital eclipse observed by INTEGRAL (Cherepashchuk et al. 2005) we found that for all models the best-fit values (corresponding to the minimum  $\chi^2$ ) are obtained for the maximum possible radius of the disk  $r_d$  and the maximum possible value of the angle  $\omega$ . This conclusion is confirmed here using new data. We also confirm that parameters  $b_j$  and  $\omega$  are correlated.

5) The minimum deviation of the best-fit model eclipsing light curve from observed points is reached for the small mass ratio  $q \sim 0.1$  and a long X-ray emitting "jet" ( $b_j > 0.5$ ) with the base radius varying in the wide range ( $r_j = 0.05 - 0.25$ ). This means that the "jet" can be long but either thin or thick. However, the main objection to model of the long "jet" comes from its inability to describe the observed precessional variability as shown in Fig. 8. We conclude that at small mass ratio  $q \leq 0.25$  our model does not simultaneously fit both orbital and precessional variability of SS433 observed by INTEGRAL. The precessional light curve could be fitted at the small mass ratio ( $q = 0.1$ ) by a short X-ray emitting "jet", but then the flux at the center of the primary eclipse would be zero (Fig. 9), again in contradiction

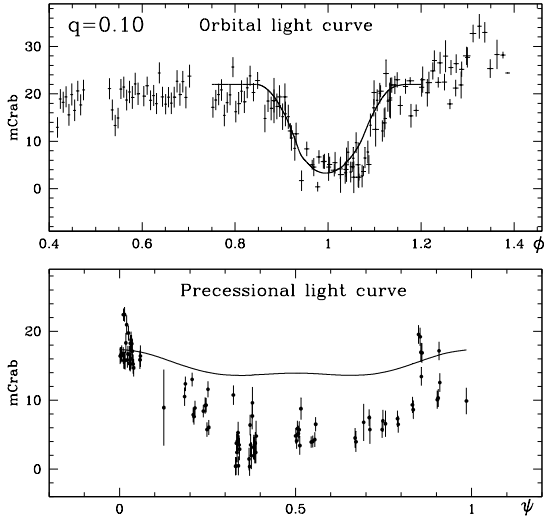


**Figure 8.** Best-fit to the orbital (top) and precessional (bottom) light curve for small binary mass ratio  $q = 0.1$  by *long* X-ray jet.

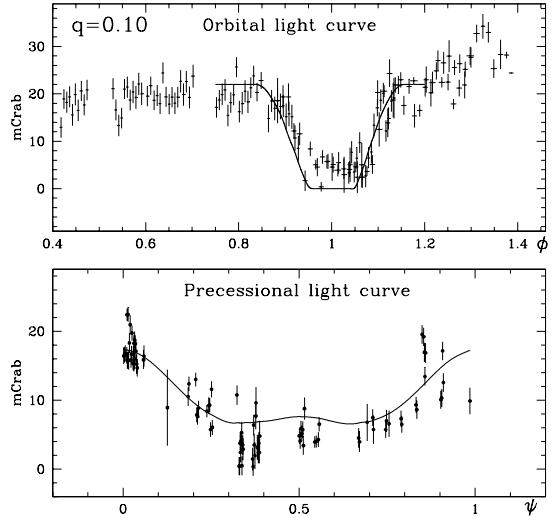


**Figure 9.** Best-fit to the orbital (top) and precessional (bottom) light curve for small binary mass ratio  $q = 0.1$  by *short* X-ray jet.

with observations – in all cases, INTEGRAL detects a non-zero X-ray flux of  $\sim 3$  mCrab at the middle of the hard X-ray eclipse (Fig. 5).

6) For  $q = 0.3 - 0.5$  our model provides almost similarly good fits to the orbital and precessional variability of SS433. To find the best-fit value of  $q$  we calculate the sum of the reduced  $\chi^2$  for the orbital and precessional light curves obtained for the same model parameters:  $\chi_{tot}^2 = \chi_{orb}^2 + \chi_{prec}^2$  (Fig. 10, panel (a)). The residuals are minimized relative to four parameters:  $r_d, \omega, r_j, b_j$ . The value  $\chi_{orb}^2$  (Fig. 10, panel (b)) corresponds to the best-fit parameters of the orbital light curve for different  $q$ . The value  $\chi_{prec}^2$  is calculated for the corresponding precessional light curve (Fig. 10, panel (c)). Fig. 10, panel (b), shows that  $\chi_{orb}^2$  deviations for the orbital eclipse increase with  $q$ ; there is a quasi-plateau at  $q \sim 0.3 - 0.5$ , then the deviations rapidly increase due to a poor fit to the orbital eclipse (especially the eclipse width, see Fig. 12). Fig. 10, panel (c), demonstrates that for  $q < 0.25$  fits to the precessional light curve sharply worsen.

As follows from Fig. 10, the values of the reduced  $\chi_{tot}^2$  and  $\chi_{orb}^2$  (minimized relative to four model parameters  $r_d, \omega, r_j, b_j$ ) are much higher than unity. This means that our model is oversimplified and is not fully adequate to the observational data. The data demonstrate a significant dispersion due to both physical variability of hard X-ray flux and systematic effects of absorption by gaseous streams and in the wind-wind collision region, which we do

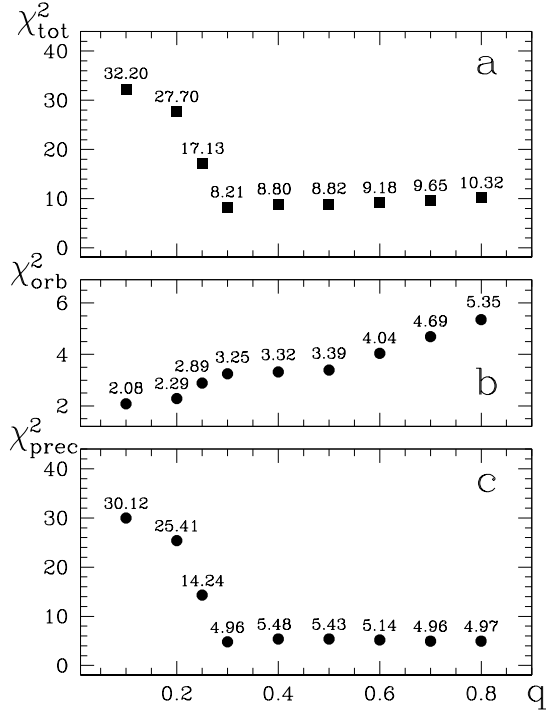


**Figure 10.** Panel a: the combined reduced  $\chi_{tot}^2 = \chi_{orb}^2 + \chi_{prec}^2$  (the sum of the  $\chi^2$  for the best-fit orbital light curve and the corresponding precessional light curve) for different  $q$ . The reduced values of orbital eclipse  $\chi_{orb}^2$  and precessional  $\chi_{prec}^2$  variability for different  $q$  are shown in panel (b) and (c), respectively. Figures mark the value of the corresponding  $\chi^2$ .

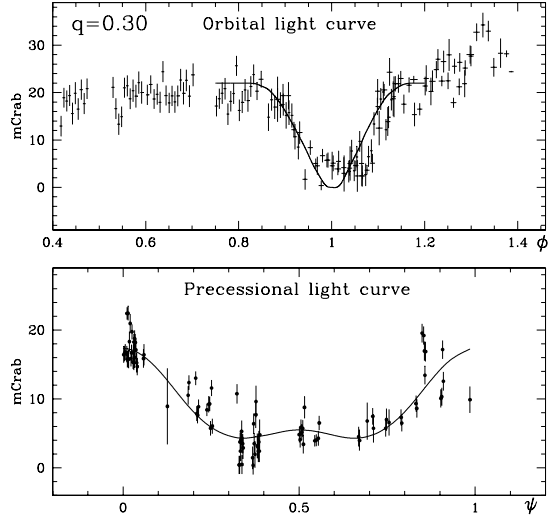


**Figure 11.** The best-fit orbital (top) and precessional hard X-ray light curve of SS433 for binary mass ratio  $q = 0.3$ .

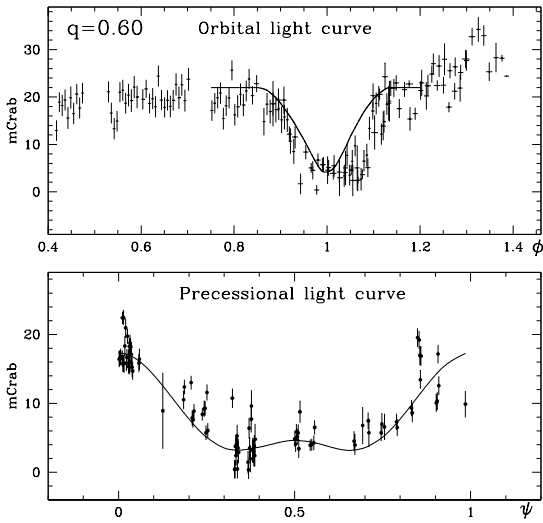


**Figure 12.** The same as in Fig. 11 for  $q = 0.6$ .

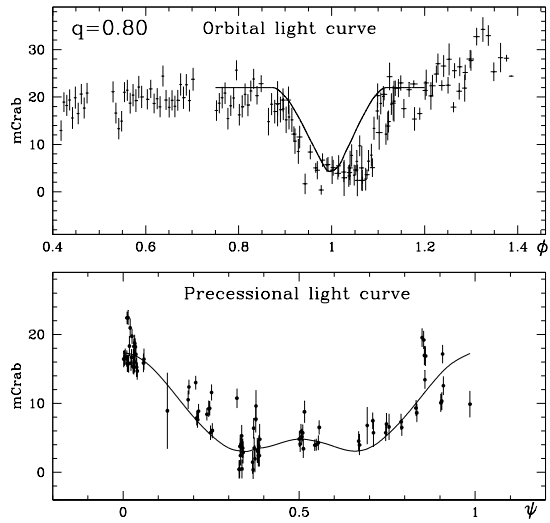


**Figure 13.** The same as in Fig. 11 for  $q = 0.8$ .

not take into account in our model. So we cannot rigorously estimate the confidence region of the sought parameter  $q$ . When the reduced  $\chi^2 > 1$ , it is generally accepted to give only the optimal value of the sought parameter, without quoting the confidence range since the latter can not be statistically justified. The absolute minimum of the residuals  $\chi_{tot}^2 \simeq 8.21$  is reached at  $q \simeq 0.3$ , so we accept it as the optimal value. Nevertheless, as the reduced residuals  $\chi_{orb}^2$  and  $\chi_{prec}^2$  strongly change with  $q$  (Fig. 10), it appears meaningful to consider the mass ratio  $q$  from the range  $\sim 0.25 - 0.5$ , where the orbital  $\chi_{orb}^2$  shows a plateau. The lower limit of the mass ratio interval is determined by the abrupt increase in the precessional  $\chi_{prec}^2$  residuals for  $q < 0.25$ , the upper limit is determined by (less abrupt) increase in  $\chi_{orb}^2$  residuals for  $q > 0.5$ .

Therefore, our simple geometrical model of SS433 suggests an acceptable range of binary mass ratio of  $0.25 \leq q \leq 0.5$ . The absolute minimum of the total reduced residuals  $\chi_{tot}^2 \simeq 8.21$  at  $q \simeq 0.3$  agrees well with the mass ratio estimate  $q \simeq 0.35$  obtained by Hillwig & Gies (2008). We stress that the latter estimate is obtained from optical spectroscopy of SS433 and is in agreement with the estimate  $q \simeq 0.4$  derived by Antokhina & Cherepashchuk (1987) from analysis of optical eclipse light curves at different precessional phases. Our new binary mass ratio estimate  $q \simeq 0.3$  is obtained from independent observations in hard X-rays. Such a good convergence of the mass ratio estimates found from different and independent observational data strengthens the reliability of the found binary mass ratio value  $q \simeq 0.3$ .

The best-fit model parameters for  $q \simeq 0.3$  (see Fig. 11) correspond to an extended oblate corona with width comparable to the size of the accretion disk ( $r_j \sim r_d$ ) and small vertical height ( $b_j \sim 0.15 - 0.20$ ). In the framework of our model, such a geometry of the hard X-ray emitting region is caused by the wide primary eclipse minimum and large amplitude of the precessional variability. The precessional light curve in hard X-rays is shaped by the outer parts of the disk eclipsing the high-temperature corona that scatters thermal X-rays from jets and possibly the innermost accretion disk (Krivosheyev et al. 2009).

Fig. 11 shows the orbital and precessional light curves for the optimal binary mass ratio  $q = 0.3$ . For comparison, best-fit model light curves for mass ratio  $q = 0.6$  and  $q = 0.8$  are presented in Fig. 12 and Fig. 13, respectively. Figs. 8, 9, 11, 12 and 13 show the change in the primary eclipse minimum width for different binary mass ratios. Clearly, the model best-fit to the form and width of the primary eclipse at  $q = 0.6$  and  $q = 0.8$  is worse than that for  $q = 0.3$ , as Fig. 10 (the middle panel) formally shows.

In Fig. 14 we illustrate the view of our optimal geometrical model of SS433 with  $q = 0.3$



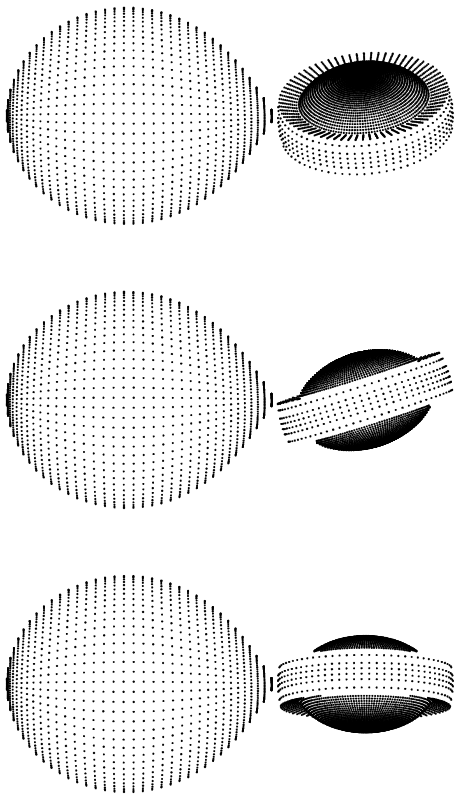


**Figure 14.** Model view of SS433 for binary mass ratio  $q = 0.3$  at different disk precession angles (15, 118, 180 degrees from top to bottom, respectively).

as seen at different precession angles. In this figure thin relativistic jets (emitting mostly in soft X-rays) are not shown.

#### 4 DISCUSSION

Our analysis confirms that SS433 is a superaccreting microquasar with black hole. The obtained high value of the best-fit binary mass ratio in SS433  $q \simeq 0.3$  allows us to explain a substantial amplitude ( $\sim 0^m.5$ ) of the optical variability at the minimum of the primary eclipse with precessional phase. The orbital inclination of SS433 is known from independent analysis of moving emission lines ( $i \simeq 78^\circ.8$ , Margon & Anderson (1989)), so at low mass ratios  $q < 0.25$  the small relative radius of the Roche lobe of the compact object should have caused the total eclipse of the bright precessing accretion disc around the compact object by the optical A7I-star, implying a constant optical flux at the center of the eclipse at different precessional phases. This contradicts observations (see e.g. Goranskij et al. (1998)). At  $q = 0.3 \div 0.5$  the size of the Roche lobe of the compact object is relatively large to cause

only partial primary optical eclipse of the accretion disc by the A7I-star at all precessional phases, which leads to a noticeable precessional variability of the minimum brightness at the middle of the primary eclipse.

A small value of the binary mass ratio was found by Kawai et al. (1989) from the analysis of soft (1 ÷ 10 keV) X-ray eclipses of SS433. The modeling of broad-band X-ray spectrum of SS433 shows that in this energy range thermal emission of relativistic jets with temperature decreasing along the jet dominates (Filippova et al. 2006; Krivosheyev et al. 2009). The observed broad width of the soft X-ray eclipse was interpreted by Kawai et al. (1989) in terms of purely geometrical model of the eclipse of jets by the optical star with sharp limb, yielding a small value of the binary mass ratio  $q = 0.15$ . The observed independence of the soft X-ray eclipse width on energy has been the main argument justifying this model and hence the inferred low value of the mass ratio. However, this argument holds only if the temperature along jets does not change with distance from the compact object. In fact it decreases along jets (unless some additional heating mechanism is assumed), so at energies  $\sim 10$  keV central parts of the jets are eclipsed. Consequently, the duration of purely geometrical eclipses must be longer at 10 keV than at  $\sim 1$  keV where cooler periphery of the jets is eclipsed (Filippova et al. 2006). The independence of the X-ray eclipse duration on energy in the 1-10 keV range can be due to the compensation of the effect of decreasing temperature along jets and the increase of soft X-ray absorption in the extended atmosphere of the optical star, which is clearly seen in the RXTE observations (Filippova et al. 2006). So the effective radius of the eclipsing star increases at lower energies. This explains the constant width of X-ray eclipse in the 1-10 keV energy range. Turning this argument around, from the independent width of the X-ray eclipse in this energy range we can conclude that the eclipsing A7I-star in SS433 has not a sharp limb, so that X-ray eclipses in SS433 are not purely geometrical and are suffered from extinction in the heavy stellar wind from the optical star. This lends additional support to our interpretation of X-ray eclipses in SS433 making use of only the upper envelope of variable eclipsing hard X-ray light curve.

Our analysis of the primary hard X-ray eclipse of SS433 at the precessional phase  $\psi \simeq 0.05$  with account for precessional variability of the off-eclipse flux suggests the optimal binary mass ratio  $q = m_x/m_v \simeq 0.3$ . From spectroscopic observations of SS433 carried out by Hillwig & Gies (2008) a semi-amplitude of the radial velocity curve of the optical A7I-component was determined:  $K_v = 58.2 \pm 3.1$  km/s. Combining it with semi-amplitude of the radial velocity curve of the compact component  $K_x = 168 \pm 18$  km/s (Hillwig et al. 2004)

and the binary inclination angle  $i = 78^\circ.8$  (Margon & Anderson 1989; Davydov et al. 2008), we obtain for the mass function of the optical component of SS433

$$f_v(m) = \frac{m_x \sin^3 i}{(1 + 1/q)^2} \simeq 0.268 M_\odot \quad (1)$$

and the spectroscopic mass ratio  $q \simeq 0.35$ . This allows us to estimate masses of the compact object and the optical star for  $q \simeq 0.3$ :

$$m_x \simeq 5.3 M_\odot, \quad m_v \simeq 17.7 M_\odot. \quad (2)$$

With the derived mass function of the compact star  $f_x(m) = 0.268 M_\odot$ , the binary mass ratio range  $q = 0.25 - 0.5$  obtained from our analysis allows the mass range of the compact star  $7.1 - 2.56 M_\odot$ . The lower mass limit for  $q = 0.5$  formally admits a neutron star as the compact object in SS433. However, the optimal value  $q \simeq 0.3$  independently obtained from the analysis of hard X-ray eclipses and precessional variability fully agrees with the mass ratio value  $q = 0.35$  found by Hillwig & Gies (2008) from optical spectroscopy. So we conclude that the compact object in SS433 is highly unlikely to be a neutron star and is indeed a black hole.

The mass of the black hole in SS433  $m_x \simeq 5 M_\odot$  is strongly based on its mass function derived from the optical spectroscopy (Hillwig & Gies 2008). The value of the mass function is very sensitive to the radial velocity semi-amplitude of the optical star  $\sim K_v^3$ . As we emphasized earlier (Cherepashchuk et al. 2005), the measured semi-amplitude can be affected by the X-ray heating effect of the optical star, since we ascribe the observed radial velocity amplitude to the center of mass of the optical star filling its Roche lobe. The effect decreases with the binary mass ratio  $q$ . Although no signatures of the X-ray illumination effect on the radial velocity amplitude was found by Hillwig & Gies (2008), the obtained semi-amplitude  $K_v$  and hence the derived mass function of the compact star in SS433 should be treated with some reservation. Clearly, new high-resolution optical spectroscopy of SS433 is in order to accurately measure the radial velocity curve of the optical star.

## 5 CONCLUSIONS

The discovery of strong variability of the hard X-ray eclipse at precessional phases corresponding to the maximum disk opening angle for the observer and regular significant precessional variability are the main findings of our INTEGRAL observations of SS433. It is shown that the duration of the primary X-ray eclipse at different epochs changes by  $\sim 2$  times, the amplitude of the precessional variability is 5-7 times. This implies that X-ray

eclipses in SS433 are not purely geometrical, they are shaped by absorption in a powerful stellar wind and gas streams from the optical star, as well as in the wind-wind collision region. So to infer the binary mass ratio  $q$  from the analysis of X-ray eclipses, we have used only the ingress to and upper envelope of egress out of the primary eclipse. The joint analysis of eclipsing light curve and the regular precessional light curve for off-eclipse flux from the system yielded the mass ratio estimate  $q \simeq 0.25 - 0.5$ . The relatively high value of the binary mass ratio  $m_x/m_v$  (and hence the relatively large size of the Roche lobe of the compact star) suggests an explanation to peculiarities of the optical variability of SS433, in particular, to the observed substantial precessional variability of the minimum brightness at the middle of the primary optical eclipse.

Using the mass function of the optical star found by Hillwig & Gies (2008)  $f_v(m) = 0.268M_\odot$  and the value of  $q = m_x/m_v \simeq 0.3$  corresponding to the absolute minimum of  $\chi_{tot}^2$  residuals, we concluded that the masses of binary components of SS433 are  $m_x \simeq 5.3M_\odot$ ,  $m_v \simeq 17.7M_\odot$ . The high mass of the compact object leaves no doubts that it is a black hole.

The independence of the hard X-ray spectrum on the accretion disk precessional phase suggests that the hard X-ray emission ( $kT = 20 - 100$  keV) is formed in an extended, hot, quasi-isothermal corona. The heating of the corona can be related to transformation of the kinetic energy of relativistic jets to an inhomogeneous wind outflow from the precessing supercritical accretion disk (Begelman et al. 2006).

The Monte-Carlo simulations of broadband X-ray spectrum of SS433 at the maximum disk opening precessional phases (Krivosheyev et al. 2009) allowed us to determine the main physical characteristics of the hot corona (temperature  $T_{cor} \simeq 20$  keV, Thomson optical depth  $\tau \simeq 0.2$ ), as well as to estimate the mass outflow rate in jets  $\dot{M}_j = 3 \times 10^{19}$  g s<sup>-1</sup> yielding the kinetic power of the jets  $\sim 10^{39}$  erg s<sup>-1</sup>.

## ACKNOWLEDGMENTS

The authors thank Dr. M. Revnivtsev for useful discussions and the anonymous referee for constructive comments. The work is partially supported by the RFBR grants 07-02-00961 and 08-02-01220.

## REFERENCES

Antokhina E.A., Cherepashchuk A.M., 1987, SvA, 31, 295

- Antokhina E.A., Seifina E.V., Cherepashchuk A.M., 1992, SvA, 36, 143
- Begelman M.C., King A.R., Pringle J.E., 2006, MNRAS, 370, 399
- Brinkman W., Kawai N., Matsuoka M., 1989, Astron. Astrophys., 218, L13
- Cherepashchuk A.M., 1981, MNRAS, 194, 761
- Cherepashchuk A.M., 1989, Sov. Sci. Rev. Ap. Space Phys., Ed. by R.A.Sunyaev, v.7, p.185
- Cherepashchuk A.M., Bychkov K.V., Seifina E.V., 1995, ApSS, 229, 33
- Cherepashchuk A.M., Sunyaev R.A., Seifina E.V., Panchenko I.E., Molkov S.V., Postnov K.A., 2003, AA, 411, 441
- Cherepashchuk A.M., Sunyaev R.A., Fabrika S.N. et al, 2005, AA, 437, 561
- Cherepashchuk A.M., Sunyaev R.A., Seifina E.V. et al, 2007, Proc. 6th INTEGRAL Workshop, eds. S. Grebenev, R.Sunyaev, C. Winkler, ESA SP-622, p. 319
- Davydov V.V., Esipov V.F., Cherepashchuk A.M., 2008, Astron. Rep., 52, 487
- Fabrika, S.N., 2004, Astrophys. Space Phys. Rev., 12, 1
- Filippova E.V., Revnivitsev M., Fabrika S., Postnov K., Seifina E., 2006, AA, 460, 125
- Gies D.R., Huang W., McSwain M.V., 2002, ApJ, 578, L67
- Goranskij V.P., Esipov V.F., Cherepashchuk A.M., 1998, Astron. Rep., 42, 209; *ibid.*, p. 336
- Hillwig T.C., Gies D.R., Huang W., McSwain M.V., Stark M.A., van der Meer A., Kaper L., 2004, ApJ, 615, 422
- Hillwig T.C., Gies D.R., 2008, ApJ, 676, L37
- Kawai N., Matsuoka M., Pan H.-C., Stewart G.C., 1989, PASJ, 41, 491
- Kotani T., 1998, PhD. The Institute of Space and Astronautical Science, Japan
- Kotani T., Kawai N., Matsuoka M., Brinkmann W., 1998, in Proc. IAU Symp. 188, eds. K. Koyama, S. Kitamoto, M. Itoh, Dordrecht: Kluwer, p. 358
- Krivosheyev Yu. M., Bisnovaty-Kogan G.S., Cherepashchuk A.M., Postnov K.A., 2009, MNRAS, 394, 1674
- Margon B., 1984, ARAA, 22, 507
- Margon B., Anderson S.F., 1989, ApJ, 347, 507
- Molkov S., Cherepashchuk A.M., Lutovinov A.A., Revnivitsev M.G., Postnov K.A., Sunyaev R.A., 2004, Astron. Lett., 30, 534
- Namiki M., Kawai N., Kotani T., Makishima K., 2003, PASJ, 55, 281
- Revnivitsev M., Burenin R., Fabrika S. et al., 2004, AA, 424, L5
- Revnivitsev M., Fabrika S., Abolmasov P. et al., 2006, AA, 447, 545

Shakura N.I., Sunyaev R.A., 1973, AA, 24, 337